# A Hybrid Radial Bearing with Improved Rotordynamic Stability

**Luis San Andrés**
*Mechanical Engineering Department*
*Texas A&M University*
*College Station, TX 77843-3123*

## ABSTRACT

Process fluid hybrid (hydrostatic/hydrodynamic) bearings find numerous applications in high performance turbomachinery operating under severe environmental constraints. Hybrid cryogenic liquid bearings currently replace ball bearings in space propulsion turbopumps due to their high stiffness and damping characteristics derived from the turbulent fluid flow through the bearing film lands induced by the high rotational speeds and large pressure differentials. Extensive analytical and experimental research has shown that hybrid bearings are prone to show two types of dynamic instabilities. Operation with compressible fluids could lead to pneumatic hammer if the bearing recesses and feed restrictor and supply line are not properly designed. Operation at high rotor speeds, on the other hand, generates large cross-coupled forces and induces a hydrodynamic instability characterized by rotor whirl at subsynchronous frequencies, typically 50% of the rotor speed. This instability cannot be easily removed within the constraints of a rigid bearing geometry, except for angled injection against rotation, adequate only for low to moderately high rotor speeds. A hybrid bearing geometry allowing stable operation at larger rotor speeds than with conventional multi-pocket hybrid bearings is presented. The rudiments of the analysis are highlighted followed by a discussion on computed results (force coefficients and leakage) for the novel bearing and a conventional one in a cryogenic turbo pump application. The novel design exploits the features of geometric asymmetry and recess (pocket) positioning to produce a bearing with a low whirl frequency ratio while still maintaining adequate levels of direct stiffness and damping coefficients. Experimental results conducted on a water lubricated hydrostatic bearing facility at TAMU have fully confirmed the advantages of the novel bearing.

**Keywords:** Fluid film bearings, rotordynamic instability

## INTRODUCTION

Hydrostatic bearings derive their load capacity not from shear flow driven effects (hydrodynamic wedge) but rather from the combination of pressure versus flow resistance effects through a feed restrictor and within the bearing film lands. Hydrostatic bearings can support large loads without journal rotation, have low friction and wear, and provide large (accurate and controllable) direct stiffness and good damping coefficients. Note that hydrostatic bearings require an external pressurized supply system and some type of flow restrictor. Also, under dynamic motions, hydrostatic bearings may display a pneumatic hammer effect due to fluid compressibility. However, and most importantly,

the load and static stiffness of a hydrostatic bearing are independent of fluid viscosity; thus making this bearing type very attractive for cryogenic liquid or low viscosity process fluid applications, further satisfying severe environmental constraints. Hybrid (combination hydrostatic and hydrodynamic) journal bearings *(HJBs)* enable smaller and lighter turbo pumps through no bearing DN life limitation and no sub-critical rotor operation [1-6].

Primary power cryogenic turbo pumps operate at high speeds (~ 170 krpm) and produces large fluid pressure rises (max. 30 MPa). These typical operating conditions determine the flow in the supporting fluid film bearings to be fully turbulent with dominance of fluid inertia and thermal transport effects. San Andrés [1-6] published bulk-flow analyses and computational programs for the prediction of the static and dynamic forced response of *HJBs* and damper seals. More than 30 hybrid journal bearings and damper seals with rotational speeds ranging from 10 to 25 krpm and pressure differentials from 4 to 7 MPa have been tested for their rotordynamic force coefficients, leakage and load capacity at a water lubricated, high-speed Hydrostatic Bearing Test Facility [7-13]. Extensive comparisons show the bulk-flow model predictions correlate favorably with the experimental results. Accurate predictions depend greatly on the knowledge of the bearing operating clearances, and most importantly, on the orifice discharge coefficients. The references cited also discuss the sensitivity of the computed predictions to variations in the input empirical parameters [8-13].

Despite the many advantages offered by *HJBs*, rotordynamic instabilities due to hydrodynamic (shear flow) and "pneumatic hammer" effects are issues of primary concern for high speed operation with large pressure differentials. Pneumatic hammer effects are avoided by appropriate selection of the flow restrictor, by designing bearing recesses with small volumes, and by restricting bearing operation to flow conditions where the pressure differential is a small fraction of the liquid bulk modulus [14].

Severe sub synchronous vibrations at rotational speeds above a certain threshold denote a hydrodynamic instability on rotor-fluid film bearing systems and due to the effect of journal rotational speed on the shear flow field. This condition is typical of fixed geometry bearings. The threshold speed corresponds to the rotor speed at which a bearing is deprived from its effective damping and any small perturbation from an equilibrium position will determine unbounded rotor motions. The whirl frequency ratio *(WFR)* denotes the ratio between the whirl frequency (typically the system first critical speed) and the threshold speed of instability. Plain journal bearings show a *WFR* equal to 0.50 for small to moderate operating eccentricities (light loads), and thus instability onsets at rotational speeds equal to twice the system first critical speed. Measurements in hybrid bearings verify closely the theoretical *WFR* prediction. In some circumstances the *WFR* even increases above 0.50, in particular for low rotational speeds and large supply pressures [9-11]

The half frequency whirl condition severely limits the application of *HJBs* in high speed, light weight turbomachinery, and thus concerted efforts have been directed towards conceiving (fixed geometry) hybrid bearings with improved stability characteristics, and

without loss in centering stiffness and damping ability. Some of the technological advances evolved from analysis and engineering design, while others followed empiricism and well known past experiences. The recommended fixes to improve the hydrodynamic stability of hybrid bearings by reducing or eliminating the *WFR* are:

- Roughen bearing surfaces to decrease the cross-coupled stiffness coefficients. Test results in a rough knurled-pattern *HJB* showed a *WFR* as low as 0.30 but with a reduced load capacity and direct stiffness when compared to a smooth surface *HJB* [9].

- Flexure-pivot, tilting pad *HJBs* due to their inherent stability. San Andrés [5] introduces the analysis and fully evaluates their potential for cryogenic uses. Flexure-pivot *HJBs* constitute a novel alternative and full-scale testing demonstrated the expected performance.

- Hybrid bearings with angled liquid injection opposing journal rotation to reduce the development of the circumferential flow velocity and virtually eliminate cross-coupled stiffness coefficients. This concept, although lacking firm theoretical modeling, has proven successful in some applications [15]. Experimental measurements for a 5 recess water HJB demonstrate that angled injection aids in reducing the whirl frequency ratio without decreasing the bearing centering stiffness and load capacity [11, 12, 13].

- Circumferentially asymmetric pad bearings to produce anisotropy in the rotordynamic force coefficients [3]. This concept and its analysis are detailed next. A conventional 360° *HJB* with an even number of recesses ($N_{rec}$) is split into two pad hydrostatic bearings with axial grooves separating the bearings, each with ½ $N_{rec}$ recesses per pad. This simple change increases the stable operating speed range of a conventional *HJB,* in particular for applications where fluid compressibility severely degrades bearing forced performance. The novel design enhances stability by providing a lower direct stiffness in the plane of the axial grooves as compared to the orthogonal stiffness.

**ANALYSIS**

Figure 1a shows the geometry of a conventional (360° extent) hybrid journal bearing. A liquid at high pressure ($P_s$) and inlet temperature ($T_s$) is supplied radially through orifice restrictors and enters into the bearing recesses with a mean pressure ($P_R$). The pressure field within the recesses is determined from flow continuity with the film lands, momentum exchange at the orifice plane and a viscous rise due to journal rotation. At the recess edges, an inertial pressure drop also occurs due to the sudden transition from the recess of depth ($H_R$) into the film lands of thickness ($H$), see Figure 2. Past the recesses, the liquid then flows through the film lands and the pressure drops to the discharge value ($P_a$).

Figure 1b shows the innovative *HJB* geometry with axial grooves (180° apart) effectively dividing the cylindrical bearing into two arcuate pads. The discharge pressure at the deep grooves effectively breaks the rotational symmetry of the bearing. This configuration is essential to provide, at the journal centered position, an asymmetry in the dynamic force coefficients that should reduce the whirl frequency ratio.
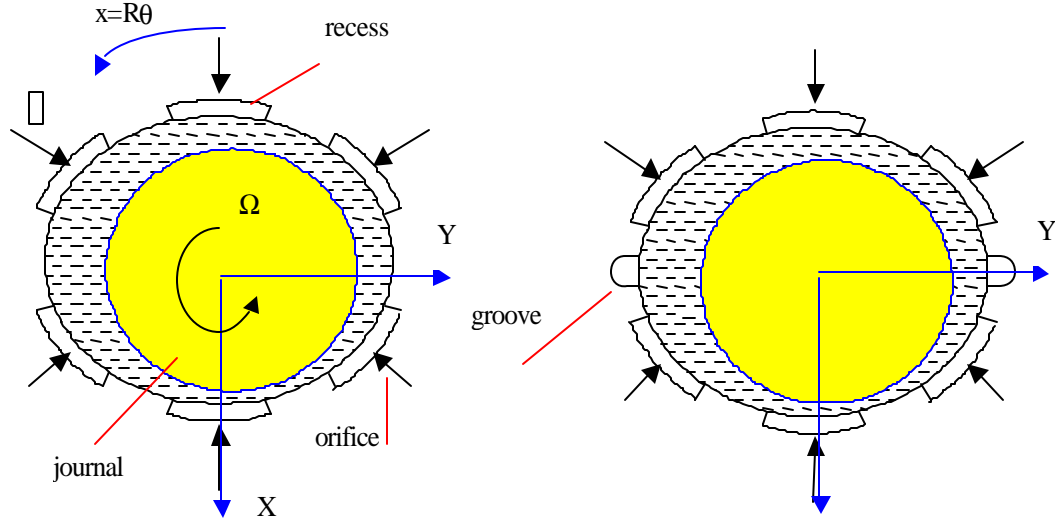
**Figure 1. Geometry of radial hydrostatic journal bearing (a) conventional design, (b) two pad grooved with asymmetric recesses.**

## Bulk-flow equations in the film lands

The model considers the fully developed turbulent bulk-flow of a fluid whose material properties depend on its local thermophysical state of pressure and temperature. The general transport equations including these features are [6]:

$$\frac{\partial(\boldsymbol{r}H\boldsymbol{y})}{\partial t}+\frac{\partial(\boldsymbol{r}HU_{x}\boldsymbol{y})}{\partial x}+\frac{\partial(\boldsymbol{r}HU_{y}\boldsymbol{y})}{\partial y}=S \tag{1}$$

| where | Variable | Source term, $S$ |
|---|---|---|
| conservation of mass equation | $\boldsymbol{y}=1$ | $0$ |
| transport of circumferential momentum velocity | $\boldsymbol{y}=U_x$ | $-H\dfrac{\partial P}{\partial x}-\dfrac{\boldsymbol{m}}{H}\left(\boldsymbol{k}_x U_x-\boldsymbol{k}_J\dfrac{\Omega R}{2}\right)$ |
| transport of axial momentum velocity | $\boldsymbol{y}=U_y$ | $-H\dfrac{\partial P}{\partial y}-\dfrac{\boldsymbol{m}}{H}\left(\boldsymbol{k}_y U_y\right)$ |

The film thickness $(H)$ is a function of the nominal clearance $(c)$ and journal center eccentricity $(e_{X,Y})$, i.e.

$$H=c(\boldsymbol{q})+e_X\cos\boldsymbol{q}+e_Y\sin\boldsymbol{q} \tag{2}$$

The wall shear stress parameters $\boldsymbol{k}_y=\boldsymbol{k}_x=\tfrac{1}{2}(\boldsymbol{k}_J+\boldsymbol{k}_B)$ with $\boldsymbol{k}_J=f_J R_J$, $\boldsymbol{k}_B=f_B R_B$, and the friction factors $(f_{J,B})$ depend on the bearing and journal surface conditions and the flow Reynolds numbers relative to the rotating $(R_J)$ and stationary $(R_B)$ surfaces [16]. The cryogenic liquid properties are extracted from the Benedict-Web-Rubin equation of state [17].

The fluid pressure equals the specified ambient value $(P_a)$ at the bearing sides $(y=\pm L/2)$ and at the leading and trailing edges of a bearing pad. Other formulae accounting for (inertial) pressure recoveries at the discharge planes or a ram pressure at the pad leading edge are not presented for brevity. At the interface with the bearing recesses, continuity of flow and pressure must be attained as detailed below.

**Flow and pressure equations at a bearing recess**

Figure 2 depicts a bearing recess with axial length $(l)$ and circumferential extent $(b)$. The recess area $A_R = l\, b$, and the feed orifice has diameter $d_o$ with a feed volume equal to $V_{supply}$. The simplified analysis of hydrostatic bearings does not model the flow field within the recess since these are (typically) deep and enclose a nearly stagnant large fluid volume. The present model accounts only for flow continuity with the film lands and sets the recess pressures $(P_R)$ from the well-known orifice flow equation implementing an empirical discharge coefficient $(C_d)$. Hill et al. [18] discuss the complexity of the flow field in hydrostatic pockets as determined from CFD studies. Their numerical results reveal the generation of hydrodynamic pressures within the pocket followed by sharp inertial pressure drops at the recess edges.
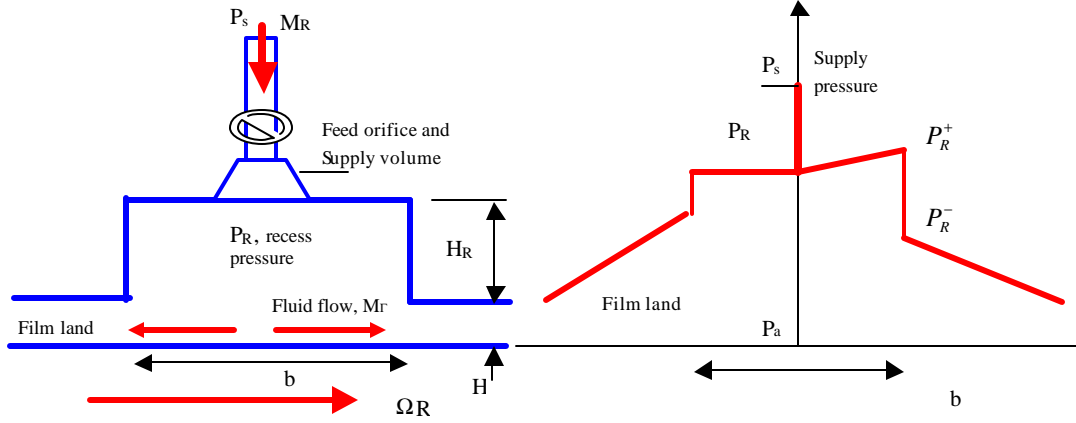


**Figure 2. Hydrostatic recess geometry and pressure distribution.**

The continuity equation at a hydrostatic recess establishes a balance among the mass flow through the feed orifice $(M_R)$, the flow through the boundaries of the recess into the film lands $(M_\Gamma)$, and the accumulation of fluid mass within the recess volume, $V_R=[A_R (H+H_R)+V_{supply}]$. That is,

$$M_R = C_d\, A_o \left( \frac{\rho}{2}[P_s - P_R] \right)^{1/2} = M_\Gamma + \frac{\partial}{\partial t}\left( \rho V_R \right) \tag{3}$$

where $M_\Gamma = \oint \rho\, H\, \vec{U}\, \hbar\, d_\Gamma$, $A_o = C_d \rho d_o^2/4$ is the effective orifice area, and $\mathbf{G}$ denotes the closure of the recess with the film lands and has a normal $\mathbf{h}$ along the boundary line.

The circumferential pressure downstream of the feed orifice $(P_R^+)$ is given, as in a Rayleigh step bearing, by

$$P_R^+ = P_R + \boldsymbol{m}\boldsymbol{k}_x \frac{b}{2(H+H_R)^2}\left\{\frac{\Omega R}{2}-U_x\right\}_R \tag{4}$$

Fluid inertia causes a sudden pressure drop at the interface between a recess and the film lands. The entrance pressures $(P_R^-)$ to the film lands bounding a recess are given by,

$$\left\langle P_R^- = P_R^+ + \frac{(1+\boldsymbol{x})}{2}\boldsymbol{r}\left[1-\left(\frac{\overline{\boldsymbol{r}}_e^-}{\overline{\boldsymbol{r}}_e^+}\right)\left(\frac{H}{H+H_R}\right)^2\right]U_{x,y}^2\right\rangle_{i=1,...,N_{rec}} \tag{5}$$

where $(\boldsymbol{x})$ represents empirical entrance loss coefficients at the recess edges. The sudden pressure drop is accounted for only if the fluid flow effectively enters the thin film lands.

**Perturbation analysis**

Small amplitude radial journal motions $(\Delta X, \Delta Y)$ about an equilibrium position $(e_{Xo}, e_{Yo})$ allow expressing the film thickness and flow variables as the superposition of equilibrium and perturbed flow fields, i.e.

$$H = H_0 + (\Delta X \cos \boldsymbol{q} + \Delta Y \sin \boldsymbol{q})e^{i\boldsymbol{w}t};$$
$$\boldsymbol{y} = \boldsymbol{y}_0 + (\Delta X \boldsymbol{y}_X + \Delta Y \boldsymbol{y}_Y)e^{i\boldsymbol{w}t}; \tag{6}$$
$$\boldsymbol{y} = \{P, U_x, U_y, \boldsymbol{k}_J, \boldsymbol{k}_B\}$$

where $(\boldsymbol{w})$ is an excitation frequency and $\boldsymbol{i}=(-1)^{1/2}$. Substitution of the fields above into the transport equations in the film lands and recesses renders sets of zeroth- and first-order flow equations for evaluation of the bearing static load capacity, drag torque, recess flow rates and dynamic force coefficients. San Andrés [1-6] details in full the procedure and resulting equations.

**Numerical Method of Solution**

The computational method for solution of the transport equations in the film lands coupled to the recess flow equations implements the control-volume CFD scheme of Launder and Leschziner [19] and the SIMPLEC procedure of Van Doormaal and Raithby [20]. Staggered grids containing control volumes for the primitive flow variables (circumferential and axial velocity, pressure and temperature) cover the flow domain. Satisfaction of the recess mass flow constraint is ensured through a Newton-Raphson scheme. San Andrés [1-6] discusses the method and its accuracy, its extension to compressible fluids and complex geometries, and parametric studies to determine the sensitivity of rotordynamic force predictions to variations in input (usually known) parameters and empirical coefficients.

Fluid film forces *(F)* and rotordynamic force coefficients are determined from integration of the equilibrium and first-order pressure fields acting on the journal surface, i.e.

$$F_a = \iint P_0 \, h_a \, dx \, dy; \quad ab=X,Y$$
$$K_{ab} - \boldsymbol{w}^2 \, M_{ab} + i \, \boldsymbol{w} \, C_{ab} = \iint P_b \, h_a \, dx \, dy; \tag{7}$$

with $\{h_X = \cos\boldsymbol{q}, h_Y = \sin\boldsymbol{q}\}$. The bearing equivalent stiffness and whirl frequency ratio are calculated using the formulae [21],

$$K_{eq} = \frac{K_{XX}C_{YY} + K_{YY}C_{XX} - C_{YX}C_{XY} - C_{XY}C_{YX}}{C_{XX} + C_{YY}} = M_{crit}\,\boldsymbol{w}_s^2 \tag{8a}$$

and

$$WFR = \left(\frac{\boldsymbol{w}_s}{\Omega_s}\right)^2 = \frac{\left(K_{eq} - K_{XX}\right)\left(K_{eq} - K_{YY}\right) - K_{XY} \cdot K_{YX}}{\left(C_{XX}C_{YY} - C_{XY}C_{YX}\right)\Omega} \tag{8b}$$

for relatively small inertia force coefficients.

## DISCUSSION OF PREDICTED RESULTS

Table 1 lists the geometry and operating conditions of a six recess *HJB* bearing for application in a Liquid Hydrogen turbo pump. Predictions are presented for (1) a conventional 360∘ bearing, and (2) the novel configuration with the bearing divided into two pads of 165∘ extent and asymmetrically positioned recesses.

Figure 3 shows the leakage and torque for both bearings versus increasing journal eccentricities, ($e_X$) towards the middle of the bottom recess and ($e_Y$) orthogonal towards the grooves. Figure 4 depicts the dimensionless bearing reaction load $\left(F / LD[P_s - P_a]\right)$ as a function of the journal eccentricity. The predictions show the novel *HJB* with grooves does not greatly affect the static load performance nor increase the leakage rate.
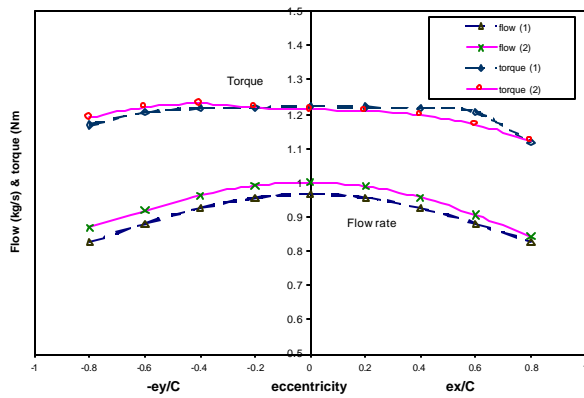


**Figure 3. Flow rate and torque for LH2 HJB vs. journal eccentricity. (1) 360 deg bearing (2) modified 2-pad HJB**
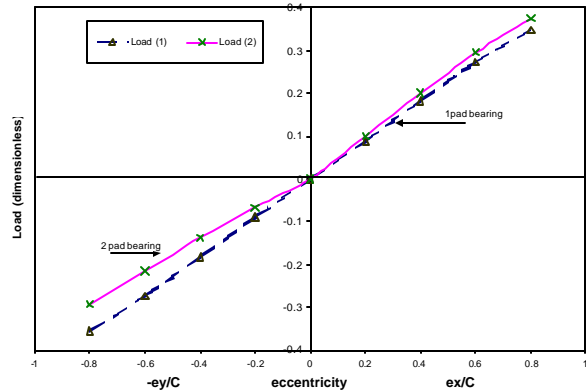
**Figure 4. Dimensionless load capacity for LH2 HJB vs. journal eccentricity. (1) 360 deg bearing (2) modified 2-pad HJB**

## Table 1. Hydrostatic bearing for LH2 turbo pump

Radial injection at mid plane of a recess.

| Geometry, $N_{rec}$=6 | | | Operating conditions | | |
|---|---|---|---|---|---|
| Diameter | $D=2R$ | 92.7 mm | Speed (25 krpm) | $\Omega$ | 2,618 rad/s |
| Length | $L$ | 37.1 mm | Supply temperature | $T_s$ | 44.6 ∘ K |
| Clearance | $C$ | 0.076 mm | Supply pressure, | $P_s$ | 267 bar |
| Recess axial length | $l$ | 19.0 mm | Exit pressure | $P_a$ | 88.1bar |
| Recess arc length *(b/R)* | $\Theta_R$ | 24 ∘ | Fluid properties | **LH2** | |
| Recess depth | $H_R$ | 0.228 mm | Density | $r_{s,a}$ | 75, 56 kg/m$^3$ |
| Film clearance (nominal) | $C$ | 0.051 mm | Viscosity | $m_{s,a}$ | 0.00135, 0.0007 centi poise |
| Recess/Bearing area ratio | | 0.20 | Bulk modulus | $(1/b_p)$ | 777 bar |
| 2 pad bearing arc length | | 165 ∘ | TYP Circumferential Reynolds number | $Re_c$ | 58,454 |
| Orifice diameter | $d_o$ | (1) 2.48 mm (2) 2.53 mm | TYP Axial flow Reynolds number | $Re_a$ | 224,8000 |
| Empirical parameters | | | | | |
| Orifice discharge coefficient | $C_d$ | 0.80 | | | |
| Entrance loss coefficients (x,y) | | 0.0, 0.5 | | | |
| Inlet swirl coefficient | $a$ | 0.50 | | | |

Bearing and collar relative surface roughness = 0.45%

Figure 5 presents the dimensionless synchronous stiffness coefficients $\left(K_{ab}\,c/LD[P_s - P_a]\right)$ for both bearings versus the journal displacements toward the middle of a recess *(e_X)* and toward the grooves *(e_Y)*. The conventional bearing shows similar direct stiffness coefficients, $K_{XX} \sim K_{YY}$, for small to moderate journal displacements. However, the grooved *HJB* renders largely asymmetric stiffness coefficients, yet of significant magnitude. The cross-coupled stiffnesses are relatively small in this application dominated by axial flow effects. Nonetheless, their importance on the bearing rotordynamic instability cannot be disregarded. Note that the axial flow Reynolds number is about four times as large as the circumferential Reynolds number (see Table 1).
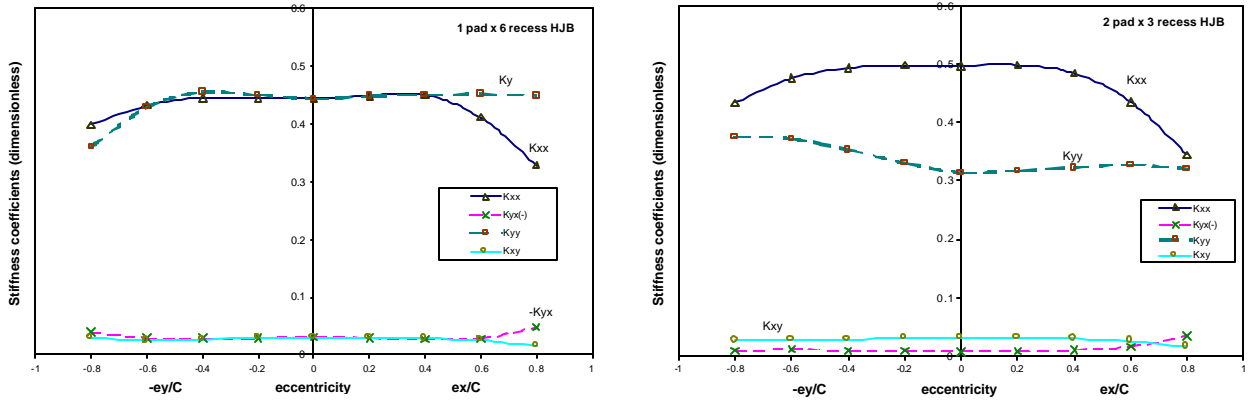


**Figure 5. Dimensionless stiffness coefficients for LH2 HJB vs. journal eccentricity. (1) 360 deg bearing (2) modified 2-pad HJB**

Figure 6 presents the dimensionless damping coefficients $\left(C_{ab}\, c\,\Omega\, /\, LD[P_s - P_a]\right)$ for both bearings. As in the case of the stiffness, the grooved *HJB* shows a direct damping coefficient *($C_{YY}$)* smaller than *($C_{XX}$)*. Note that the force coefficients remain relatively uniform for small to moderately large journal eccentricity displacements (<0.70 *c*). This linear behavior is a characteristic of well-designed hydrostatic bearings.

Inertia force coefficients are very small for $LH_2$ bearings and not shown here for brevity. This is not the case for large density fluids such as in water and liquid oxygen *HJBs* [6, 10].
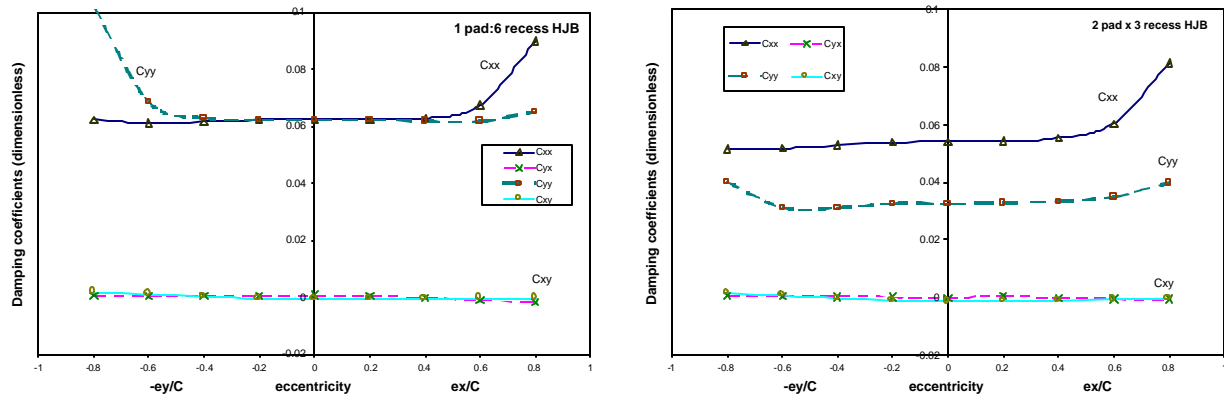


**Figure 6. Dimensionless damping coefficients for LH2 HJB vs. journal eccentricity. (1) 360 deg bearing (2) modified 2-pad HJB.**

Figure 7 shows a whirl frequency ratio *(WFR)~0.50* for the conventional cylindrical *HJB* at the journal centered position *(e~0)*. However, the grooved 2-pad *HJB* offers unlimited stability since its *WFR* is null or negative. The rationale for this important result becomes apparent when analyzing the cross-coupled stiffnesses depicted in Figure 8. The conventional bearing shows *-$K_{YX}$»$K_{XY}$* while the grooved bearing offers *-$K_{YX}$ < $K_{XY}$*. This condition enhances stability since the work brought into a whirl orbit by cross-coupled destabilizing forces is proportional to *($K_{XY}$-$K_{YX}$)* [21].

Predictions for a *HJBs* handling liquid oxygen for a cryogenic turbo pump are given in [4]. In this case, the simple two-pad *HJB* still offers a substantial reduction in *WFR* (enhanced stability) but not as pronounced as in the $LH_2$ application. Typically, $LO_2$ bearing show dominance of hydrodynamic effects due to the large fluid density and reduced operating clearances to keep the flow rate within desired rates. Proprietary experimental results conducted for Rockwell at the water hydrostatic bearing facility at Texas A&M University have fully confirmed the advantages of the novel bearing and secured the usability of the patented design.
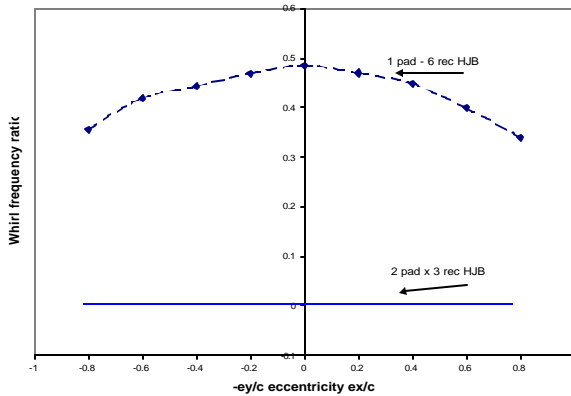
Figure 7. Whirl frequency ratio for LH2 HJB vs. journal eccentricity. (1) 360 deg bearing (2) modified 2-pad HJB
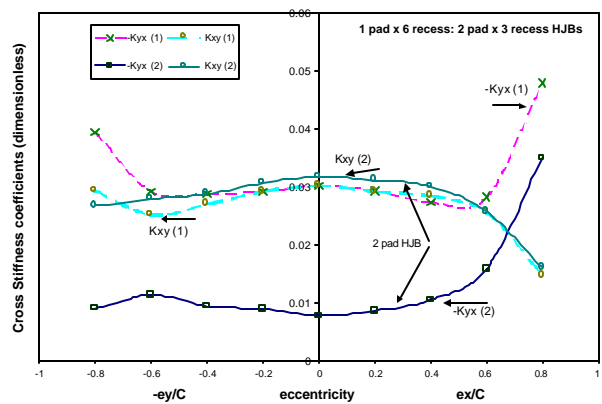


Figure 8. Cross-coupled stiffness coefficients for LH2 HJB vs. journal eccentricity. (1) 360 deg bearing (2) modified 2-pad HJB

## CLOSURE

Modern turbomachinery operating at high speeds and large pressures incorporate process fluid hybrid (hydrostatic/hydrodynamic) journal and thrust bearings to reduce the number of parts, to eliminate expensive mineral lubricant storage and pumping, thus also satisfying stringent environmental constraints.

Extensive analytical and experimental research has brought forward the technology of hybrid journal bearings *(HJBs)* for advanced turbo pump applications. Computational analyses including flow turbulence, fluid inertia and compressibility and thermal effects have been advanced to address the unique needs of the technology. The analyses have been validated by careful experimentation with measurements of load, leakage and torque, and identification of rotordynamic force coefficients. Fixed geometry *HJBs,* however, do have limited stability characteristics with a whirl frequency ratio (*WFR*) ~0.50, like plain hydrodynamic journal bearings. Thus, investigations have been underway to eliminate this limiting operating condition.

The analysis of an axially grooved two pad *HJB* shows promising results that significantly enhance its hydrodynamic stability as evidenced by the predicted low *WFR*. The engineered asymmetric geometry renders a pronounced asymmetry in the dynamic force coefficients. The innovative *HJB* still offers nearly identical torque, load capacity and flow rate, and principal direct stiffnesses when compared to a conventional cylindrical *HJB*.

The axially-grooved two-pad *HJB* shows remarkably good dynamic stability operating conditions for operating conditions with dominance of hydrostatic effects, and effectively counteracts the deleterious effects of hydrodynamic shear flow and liquid compressibility at the recess volumes. The novel bearing offers a promising alternative, as easy to

manufacture as the conventional *HJB*, and much less expensive than other proposed *HJB* designs with improved stability characteristics (angled injection, roughened surfaces or tilting pads).

**REFERENCES:**

1. San Andrés, L.A., Turbulent Hybrid Bearings with Fluid Inertia Effects, *J. of Trib., Trans. ASME,* Vol. 112, (1990) 699-707.
2. San Andrés, L., Analysis of Turbulent Hydrostatic Bearings with a Barotropic Fluid, *J. of Trib., Trans. ASME,* Vol. 114, (1992) 755-765.
3. San Andrés, L., Thermohydrodynamic Analysis of Fluid Film Bearings for Cryogenic Applications, *AIAA Journal of Propulsion and Power*, Vol. 11, No. 5 (1995) 964-972.
4. San Andrés, L., Two Pad Axially Grooved Hydrostatic Bearing, U.S. Patent 5,433,528, July 18 (1995).
5. San Andrés, L., Turbulent Flow, Flexure-Pivot Hybrid Bearings for Cryogenic Applications, *J. of Trib., Trans. ASME,* Vol. 118, No. 1, (1996) 190-200.
6. Yang, Z., L. San Andrés and D. Childs, Thermohydrodynamic Analysis of Process Liquid Hydrostatic Bearings in Turbulent Regime, *J. of Applied Mech., Trans. ASME,* Vol. 62, No. 3, (1995) 674-684.
7. Childs, D., and K. Hale, A Test Apparatus and Facility to Identify the Rotordynamic Coefficients of High Speed Hydrostatic Bearings, *J. of Trib., Trans. ASME,* Vol. 116, (1994) 337-344.
8. Kurtin, K., Childs, D., San Andrés, L. and Hale, K., Experimental versus Theoretical Characteristics of a High Speed Hybrid (combination Hydrostatic and Hydrodynamic) Bearing, *J. of Trib., Trans. ASME,* Vol. 115, No. 1, (1993) 160-169.
9. Franchek, N., and D. Childs, Experimental Test Results for Four High-Speed, High-Pressure, Orifice-Compensated Hybrid Bearings, *J. of Trib., Trans. ASME,* Vol. 116, No. 2, (1994) 285-290.
10. Mosher, P., and D. Childs, Theory Versus Experiment for the Effect of Pressure Ratio on the Performance of an Orifice-Compensated Hybrid Bearing," ASME Design Engineering Technical Conference, DE-Vol 84-2, Vol.3-Part B, (1994) 1119-1129.
11. Franchek, N., D. Childs, and L. San Andrés, Theoretical and Experimental Comparisons for Rotordynamic Coefficients of a High-Speed, High-Pressure, Orifice-Compensated Hybrid Bearings, *J. of Trib., Trans. ASME,* Vol. 117, No. 2, (1995) 285-290.
12. San Andrés, L., and D. Childs, Angled Injection - Hydrostatic Bearings, Analysis and Comparison to Test Results, *J. of Trib., Trans. ASME,* Vol. 119, No.1, (1997) 179-187.
13. Laurant, F., and D. Childs, Rotordynamic Evaluation of a Near-Tangential Injection Hybrid Bearing, *J. of Trib., Trans. ASME,* Vol. 121, No. 4, (1999) 886-891.
14. Redecliff, J.M. and J.H. Vohr, Hydrostatic Bearings for Cryogenic Rocket Engine Pumps, *J. of Lub. Tech., Trans. ASME,* Vol. 91, (1969) 557-575.
15. Tondl, A., Bearings with a Tangential Gas Supply, *Gas Bearing Symposium*, University of Southampton, Dept. of Mechanical Engineering (1967).
16. Hirs, G. G., A Bulk-Flow Theory for Turbulence in Lubricating Films, *J. of Lub. Tech., Trans. ASME,* Vol. 95, (1973) 135-146.
17. McCarty, R.D., NBS Standard Reference Data Base 12, Thermophysical Properties of

Fluids, MIPROPS 86, National Bureau of Standards, Colorado, 1986.

18. Hill, D., E. Baskharone, and L. San Andres, Inertia Effects in a Hybrid Bearing with a 45 degree Entrance Region, *J. of Trib., Trans. ASME,* Vol. 117, No. 3, (1995) 498-505.

19. Launder, B., and M. Leschziner, Flow in Finite Width Thrust Bearings Including Inertial Effects, *J. of Lub. Tech., Trans. ASME,* Vol. 100, (1978) 330-345.

20. Van Doormaal, J.P., and D. Raithby, Enhancements of the SIMPLE Method for Predicting Incompressible Fluid Flows," *Numerical Heat Transfer*, Vol. 7, (1984), 147-163.

21. San Andrés, Modern Lubrication Theory, Class Notes, Texas A&M University, Ch. 5, (2000). (http://metrib.tamu.edu/me626/notes)